Erik Esche, Harvey Arellano-Garcia, Lorenz T. Biegler

Optimal operation of a membrane reactor network

Optimal Operation of a Membrane Reactor Network

Erik Esche,[*,†] Harvey Arellano-Garcia,[†] and Lorenz T. Biegler[‡]

Chair of Process Dynamics and Operation, Berlin University of Technology, Sekr. KWT-9, Str. des 17. Juni 135, D-10623 Berlin, Germany, and Department of Chemical Engineering, Carnegie Mellon University, 5000 Forbes Avenue, Pittsburgh, PA 15213, USA

E-mail: erik.esche@tu-berlin.de

In honor of Günter Wozny's 65th birthday

Abstract

In this work, a two-dimensional model for a conventional packed-bed membrane reactor (*CPBMR*) is presented. The model incorporates radial diffusion and thermal conduction. In addition, two 10 cm long cooling segments for the *CPBMR* were implemented based on the idea of a fixed cooling temperature positioned outside the reactor shell. The model is discretized using two-dimensional orthogonal collocation on finite elements with a combination of Hermite for the radial and Lagrangian polynomials for the axial coordinate. Membrane thickness, feed compositions, temperatures at the inlet and for the cooling, diameters, and the amount of inert packing in the reactor are considered as decision variables. The optimization results in C_2 yields of up to 40% with a selectivity in C_2 products of more than 60%. In addition, the *CPBMR* model is integrated into a membrane reactor network (MRN) consisting of an additional packed-bed membrane reactor with an alternative feeding policy and a fixed-bed reactor.

Keywords: OCM, Membrane Reactor Network, Orthogonal Collocation, large-scale NLP

[*]To whom correspondence should be addressed
[†]Berlin
[‡]Pittsburgh

Motivation and Introduction

For remote, isolated wells of natural gas, a combination of steam reforming and Fischer-Tropsch synthesis is often applied to turn methane into more easily transportable and chemically processable hydrocarbons. However, this process demands enormous amounts of energy and has an efficiency between 25 and 50% depending on reactant compositions and operating conditions.[1] An alternative to this process is the oxidative coupling of methane (*OCM*), which has the potential to become a key technology in chemical industry.[2] The *OCM* process allows for direct production of alkenes (olefins) or alkanes from methane (CH_4). It skips the energy intensive syngas formation (steam reforming) and could thus potentially be more energetically and economically efficient. This process offers various opportunities for replacing oil with natural gas.

As part of the Cluster of Excellence "Unifying Concepts in Catalysis" (UniCat)[a], a mini-plant is being built at the Berlin Institute of Technology (Technische Universität Berlin) to investigate the technical viability of the OCM process on a larger scale. This contribution deals with the modelling and optimization of a part of that mini-plant, namely, a membrane reactor network.

Forthwith, the La_2O_3/CaO-catalyst is employed for OCM. Given the exothermic nature of OCM and the undesired simultaneous creation of carbon oxides, any practical application should allow for good temperature control and low oxygen levels. Several apparatuses like fluidized bed reactors and fixed-bed reactors (*FBR*s) have been tested therefore, where pellets in the bed carry the required catalyst. In a classical *FBR*, the equilibrium composition can ideally be attained at the outlet and the product streams need to be further processed to extract ethylene and other hydrocarbons. A more promising approach has been developed by Lafarga et al. in the form of packed-bed membrane reactors (*PBMR*s), which offer additional benefits by gradually feeding oxygen to the catalyst so as to allow for a higher selectivity in C_2 products, meaning lower carbon oxide formation.[3] *PBMR*s are comparatively simple in their process design, and safer in operation than an *FBR*.[5] They not only offer enhanced catalytic activity and selectivity, but also include the product separation.

[a] For further information on UniCat visit `http://www.unicat.tu-berlin.de`.

Nevertheless, a permeable membrane implies loss of reactants by diffusion to the non-catalytic side of the reactor. One measure, which reduces this effect, is the introduction of a recycle stream feeding a part of a product stream back into the system.[7] 1 shows the membrane reactor network (*MRN*) proposed by Godini et al.[8]

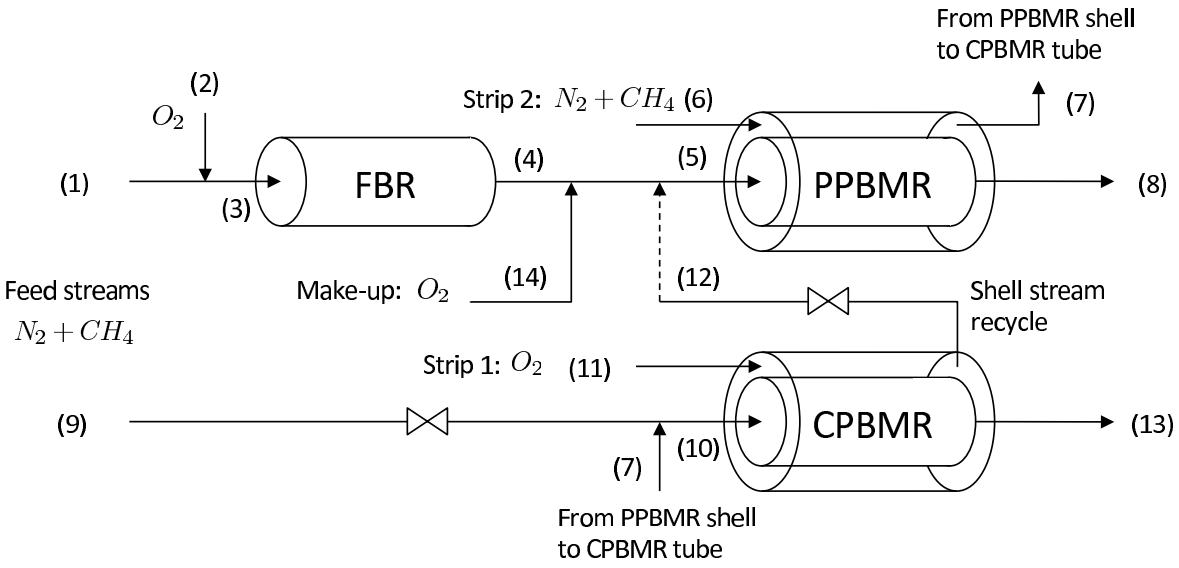

Figure 1: Flowsheet of the proposed membrane reactor network. Figure redrawn in accordance with.[8]

The network consists of three different types of reactors: a common fixed-bed (*FBR*) or plug flow reactor (*PFR*), a conventional packed-bed membrane reactor (*CPBMR*) and an alternative, proposed packed-bed membrane reactor (*PPBMR*).[8]

The foremost aim of this contribution is not to discuss the optimal structure of a membrane reactor network for the *OCM* process, but to model and optimize the operation of the given network.

In previously conducted work by Jašo and Godini et al. , only one-dimensional models for the three afore-mentioned reactors were applied to investigate the attainable reactor performance.[2 9] Their investigations of the reactor performance included the influence of operating temperature, membrane thickness, methane-to-oxygen ratio at the reactor inlet, overall feed flow rates, gas stream compositions, and reactor lengths. They saw the temperature rising especially in the *FBR* by more than 500 K despite cooling the reactor through its outer shell. Godini et al. proposed the afore-

mentioned feeding policy for the given membrane reactor network.[8] Their strategy of running a fixed-bed reactor and a conventional packed-bed membrane reactor alongside each other and connecting them both through a proposed packed-bed membrane reactor and recycles allows for an increase in both yield and selectivity. They started with separate studies of all three reactors by implementing one-dimensional stationary models to test the effect of oxygen accessibility. The *PPBMR* differs from the *CPBMR* only insofar as methane and oxygen are co-fed to the packed-bed (tube-side) of the reactor. This new feeding strategy allows for the above-mentioned network improvements. Their analyses showed an overall yield in C_2 products of 23.21%, a C_2 selectivity of 53.93%, and a methane conversion of 42.66%.

The following chapters present a brief overview on how all three reactors are modeled before discussing the simulation and optimization of the membrane reactor network.

Derivation of Models

In order to model and optimize the whole network, a model for each of the reactors has been developed. This section introduces models for all three reactors and outlines how source terms and transport coefficients are calculated. Moreover, a collocation method for a set of partial differential equations is discussed.

One- and Two-Dimensional Models: Previously implemented one-dimensional models have shown higher yields in C_2 hydrocarbons than physically possible, the focus of this contribution lies on two-dimensional modelling. The *CPBMR* is expected to have the largest impact on the behaviour of the whole network by far. Therefore, a two-dimensional model is implemented for the *CPBMR* and one-dimensional models are considered for the other two reactors. All symbols stated in the following equations are noted and explained in the nomenclature. The one-dimensional model for the FBR consists of the following differential equations describing concentration and

temperature profiles:

$$\frac{\partial c_i}{\partial z} = \frac{\dot{c}r_i}{u_z}, \tag{1}$$

$$\frac{\partial T}{\partial z} = \frac{-k_{OS} \cdot (T(z) - T_{\text{cool}}) \cdot 2 + \sum_{j=1}^{NR} \left(\varphi_{\text{cat}} \cdot \rho_{\text{cat}} \cdot \dot{r}r_j \cdot (-\Delta_R H)\right) \cdot r_{FBR}}{c_{\text{tot}} \cdot c_{p,\text{mix}} \cdot u_z \cdot r_{FBR}}. \tag{2}$$

The reactor is heated or cooled through its lateral, outer shell. T_{cool} is the temperature of the cooling jacket and k_{OS} the respective heat transfer coefficient.

For the *PPBMR* the influence of the membrane and the shell-side of the reactor need to be added to the set of differential equations. Consequently, each side has its own equations for concentrations and temperatures as follows:

$$u_{z,T} \cdot \pi \cdot r_{\text{tube}}^2 \frac{\partial c_{i,\text{ tube}}}{\partial z} \cdot dz = \dot{c}r_i \cdot \pi \cdot r_{\text{tube}}^2 \cdot dz - d\dot{N}_{i,\text{ diff}}(z) \tag{3}$$

$$u_{z,S} \cdot \pi \cdot \left(r_{\text{shell}}^2 - r_{\text{tube}}^2\right) \cdot \frac{\partial c_{i,\text{ shell}}}{\partial z} \cdot dz = d\dot{N}_{i,\text{ diff}}(z) \tag{4}$$

$$\begin{aligned} \frac{\partial T^T}{\partial z} = & \frac{\sum_{j=1}^{NR} \left(\varphi_{\text{cat}} \cdot \rho_{\text{cat}} \cdot \dot{r}r_j \cdot (-\Delta_R H)\right) \cdot \pi \cdot r_T^2}{c_{\text{tot}}^T \cdot c_{p,\text{mix}}^T \cdot u_z^T \cdot \pi \cdot r_T^2} \\ & - \frac{\dot{h}_{\text{diff}} \cdot 2 \cdot \pi \cdot r_S}{c_{\text{tot}}^T \cdot c_{p,\text{mix}}^T \cdot u_z^T \cdot \pi \cdot r_T^2} - \frac{\dot{q}_{\text{trans}} \cdot 2 \cdot \pi \cdot r_S}{c_{\text{tot}}^T \cdot c_{p,\text{mix}}^T \cdot u_z^T \cdot \pi \cdot r_T^2} \end{aligned} \tag{5}$$

$$\begin{aligned} \frac{\partial T^S}{\partial z} = & \frac{\dot{h}_{\text{diff}} \cdot 2 \cdot \pi \cdot r_S}{c_{\text{tot}}^S \cdot c_{p,\text{mix}}^S \cdot u_z^S \cdot \pi \cdot \left(r_S^2 - r_T^2\right)} + \frac{\dot{q}_{\text{trans}} \cdot 2 \cdot \pi \cdot r_S}{c_{\text{tot}}^S \cdot c_{p,\text{mix}}^S \cdot u_z^S \cdot \pi \cdot \left(r_S^2 - r_T^2\right)} \\ & - \frac{k_{OS} \cdot \left(T^S(z) - T_{\text{cool}}\right) \cdot 2 \cdot \pi \cdot r_S}{c_{\text{tot}}^S \cdot c_{p,\text{mix}}^S \cdot u_z^S \cdot \pi \cdot \left(r_S^2 - r_T^2\right)} \end{aligned} \tag{6}$$

2(a) and 2(b) show a sketch of the *CPBMR* and a differential volume element of its tube-side,

respectively. Hence, the mass balance for the tube-side leads to:

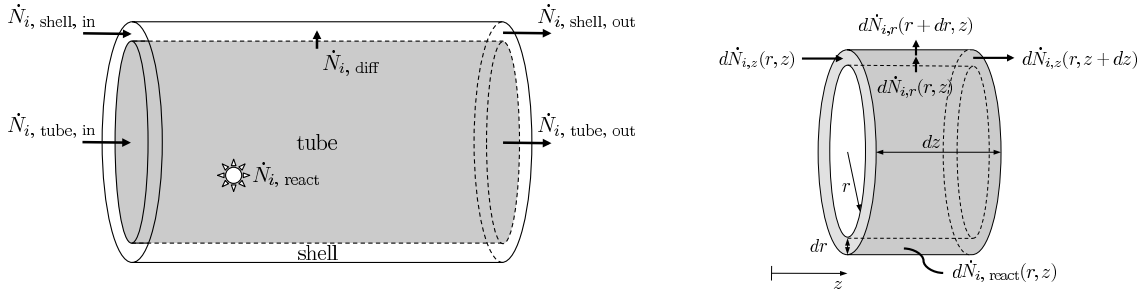

(a) Sketch of the *CPBMR* for the isothermal model.

(b) Differential segment of the tube-side of the *CPBMR* for the isothermal model.

Figure 2: Balance volume for the derivation of the isothermal model for the *CPBMR*.

$$0 = -u_z \cdot \frac{\partial c_i(r,z)}{\partial z} + \mathscr{D}_{i,r} \cdot \left[\frac{\partial^2 c_i}{\partial r^2} + \frac{1}{r} \cdot \frac{\partial c_i}{\partial r} \right] + \dot{cr}_i \tag{7}$$

and for the shell-side respectively:

$$0 = -u_z \cdot \frac{\partial c_i(r,z)}{\partial z} + \mathscr{D}_{i,r} \cdot \left[\frac{\partial^2 c_i}{\partial r^2} + \frac{1}{r} \cdot \frac{\partial c_i}{\partial r} \right] \tag{8}$$

The two-dimensional modelling moves the equations for the heat transfer through the outer shell and the membrane to the boundary conditions. A differential energy balance of the tube-side of the CPBMR leads to:

$$c_{\text{tot}} \cdot c_{p,\,\text{tot}} \cdot u_z \cdot \frac{\partial T}{\partial z} = \lambda \cdot \left[\frac{\partial^2 T}{\partial r^2} + \frac{1}{r} \cdot \frac{\partial T}{\partial r} \right] + \sum_{j=1}^{NR} \left(\varphi_{\text{cat}} \cdot \rho_{\text{cat}} \cdot \dot{r}r_j \cdot (-\Delta_R H) \right) \tag{9}$$

For the description of the shell-side, the reaction term simply needs to be left out:

$$c_{\text{tot}} \cdot c_{p,\,\text{tot}} \cdot u_z \cdot \frac{\partial T}{\partial z} = \lambda \cdot \left[\frac{\partial^2 T}{\partial r^2} + \frac{1}{r} \cdot \frac{\partial T}{\partial r} \right] \tag{10}$$

3 shows the basic idea of the heated or cooled model for the *CPBMR*. Each 10 cm segment of the

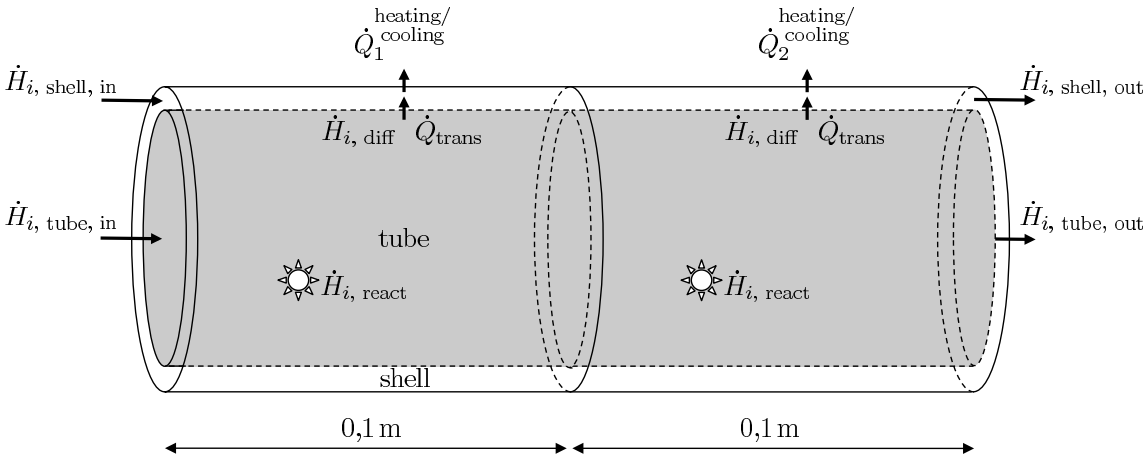

Figure 3: Sketch for the heated or cooled model of the *CPBMR*.

reactor can be cooled or heated separately through the outer shell according to:

$$\dot{q}_{\text{heat/cool}}(z) = k_{\text{OS}} \cdot \left(T(r = r_{\text{shell}}, z)\big|_{\text{shell}} - T_{\text{cool}}\right) \tag{11}$$

$$= -\lambda^{G}_{\text{mix}}(r = r_{\text{shell}}, z) \cdot \frac{\partial T}{\partial r}\bigg|_{\text{shell}} \tag{12}$$

Fluid Properties, Transport Parameters, and Reaction Kinetics: All gases are assumed to behave as perfect or ideal gases. Correlations published in[10] are employed to calculate viscosities, thermal conductivities of pure components, etc.

The shell of the *CPBMR* is void of any internal installations. Hence, it can be assumed that the radial flux in the shell is due to common gas diffusion. Fuller et al. present a semi-theoretical, semi-empirical function for the calculation of binary diffusion coefficients.[11] Using these binary diffusion coefficients, Kee et al. introduced mixture averaged diffusion coefficients, which are applied as diffusion coefficients for the shell-side of the CPBMR.[13] The packed-bed in the tube of the *CPBMR* impedes the diffusion of gas and the axial flow through the packed-bed of course affects the radial mass transport. In this contribution, an approach suggested by Tsotsas and Schlünder et al. is used, which has already been successfully applied to a packed-bed membrane reactor, in which a radial effective dispersion coefficient is defined for each component as the sum of a molecular and a crossmixing term, where the molecular term may be calculated in accordance with Kee

et al.'s correlation.[14,16]

In this work, a porous membrane, which allows the permeation of gas, separates shell- and tube-side of the *CPBMR*. The flux of any component through the membrane is calculated with the help of Kundsen's diffusivity theory as has been experimentally shown by Lafarga et al.[17] Diffusion is assumed to be the only radial transport mechanism. Therefore, the flux through the membrane of a component i on either side can also be described with Fick's law.

For the thermal conductivity of the gas mixture in the shell-side, a model presented in[18] may be used. To combine individual thermal conductivities into a single one for the whole mixture, the rule developed by Wassiljeva, Mason, and Saxena[19] is applied. Several approaches exist, which describe the effective radial thermal conductivity λ_{eff} in a packed-bed. A model for the radial thermal conduction published by Bauer and Schlünder[20,21] is employed.

Two different types of transport cause a heat flux through the membrane separating shell- and tube-side of the *CPBMR*: The diffusive mass transport brings about an enthalpy flow $\dot{h}_{\text{membrane}}$ and conduction of the membrane itself enables heat transfer $\dot{q}_{\text{membrane}}$ between both sides:

$$\dot{q}_{\text{membrane}} = k_{\text{membrane}} \cdot (T_{\text{tube}}(r = r_{\text{tube}}, z) - T_{\text{shell}}(r = r_{\text{tube}}, z)) \tag{13}$$

$$\dot{h}_{\text{membrane}} = \sum_{i=1}^{NC} \left(\dot{n}_{i,\,\text{diff}} \cdot c_{p,i}\right) \cdot (T_{\text{tube}}(r = r_{\text{tube}}, z) - T_{\text{shell}}(r = r_{\text{tube}}, z)) \tag{14}$$

Specchia et al.[22]published correlations for the calculation of heat transfer coefficients for heat transfer through walls adjoining catalytic packed-beds. For the one-dimensional case, a different approach is required as there are no temperature gradients on either side of the membrane. Dixon[23] developed correlations for the latter case. Moreover, the kinetic model of Stansch et al. for the oxidative coupling of methane over a La_2O_3/CaO-catalyst is used in this work. Their reaction mechanism is detailed in.[24]

Orthogonal Collocation for Reactor Models: All differential equations in this contribution are discretized via orthogonal collocation on finite elements. Third order Lagrangian polynomials are

employed to collocate ODEs (ordinary differential equations) on finite elements using Radau roots to guarantee the continuity of each variable across finite elements.[26]

For partial differential equations (PDEs) a combination of Hermite and Lagrangian polynomials is derived for the descretization. In case second order derivatives appear in a differential equation, the continuity of first order derivatives across finite elements needs to be ensured. For this application, Hermite cubic polynomials are of advantage. Their usage guarantees the continuity of the function itself and its first derivative between two adjoining finite elements. The polynomials employed forthwith are taken from Finlayson, who used Hermite polynomials for the two-dimensional discretization of a sphere.[28]

The basic idea of extending the one-dimensional orthogonal collocation to a second dimension is to use different functions for each direction, which depend on different variables and then multiply both of them.

$$c_{LH}(u,v) = \left(\sum_{l=1}^{4} a_{u,l} \cdot \ell_l(u)\right) \cdot \left(\sum_{l=1}^{4} a_{v,l} \cdot \mathscr{H}_l(v)\right) \tag{15}$$

Equation 15 can also be written as follows where $a_{i,j} = a_{u,i} \cdot a_{v,j}$:

$$c_{LH}(u,v) = a_{1,1} \cdot \ell_1(u) \cdot \mathscr{H}_1(v) + a_{1,2} \cdot \ell_1(u) \cdot \mathscr{H}_2(v) + a_{1,3} \cdot \ell_1(u) \cdot \mathscr{H}_3(v) \tag{16}$$

$$+ a_{1,4} \cdot \ell_1(u) \cdot \mathscr{H}_4(v) + a_{2,1} \cdot \ell_2(u) \cdot \mathscr{H}_1(v) + \ldots + a_{4,4} \cdot \ell_4(u) \cdot \mathscr{H}_4(v) \tag{17}$$

The new approximation function, which is basically a surface function, contains 16 coefficients $a_{i,j}$, half of which assume the value of the collocated variable at certain collocation positions and the other half are the respective first, radial derivative. This is depicted in 4.

Application of Orthogonal Collocation to Reactor Models: The two-dimensional model for the *CPBMR* is discretized using orthogonal collocation as described above. Hence, the *CPBMR* displayed in 2(a) needs to be divided into several axial and radial finite elements. The following scheme is applied to formulate a linearly independent set of equations based on the discretized differential equations: The assessment of each stand-alone reactor and the network is done using

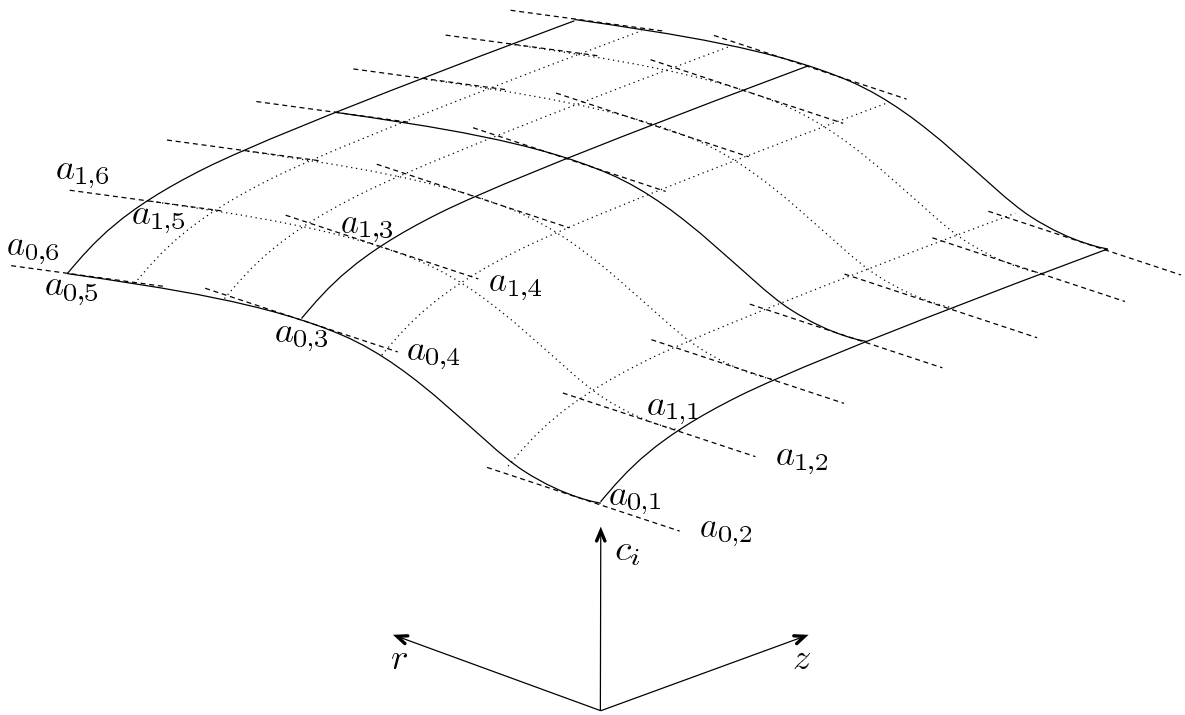

Figure 4: Depiction of the collocating surface function using Hermite and Lagrangian polynomials and the meaning of respective collocation variables.

Godini et al.'s[8] definitions of yield Y, selectivity S in C_2 hydrocarbons, and CH_4 conversion X.

In order to solve the resuling NLP problem , the interior point barrier method implemented in IPOPT is used. For details see Biegler et al.[29,30]

Stand-Alone Operation of the *CPBMR*

Preceding the optimization, extensive simulation studies are carried out. To accurately simulate the CPBMR, three radial finite elements for the tube-side, two for the shell-side, and twelve axial finite elements are required. By making each of the aforementioned model parameters in turn dependent on local concentrations and temperatures, it could be found that all fluid properties and transport coefficients should in fact not be calculated with averaged concentrations and temperatures, but using locally dependent values. Relative errors of mass and atom balances are below 10^{-5}. Ignoring the heat of reaction or the influence of the heat loss through the outer shell can have a big impact on

the performance. Non-isothermal models should be preferred at all times. A comparison between the two-dimensional and a one-dimensional model shows an overestimation of the reactor performance in terms of yield in C_2 hydrocarbons by as many as 25 percentage points. The full-scale model for the CPBMR consists of around 160 000 variables. Due to the reaction kinetics and some of the correlations for transport parameters, the entire system is highly non-linear. Consequently, a number of measures is tested to improve the convergence behaviour of the entire system such as avoiding non-differentiable points, scaling of variables (e.g. using natural logarithms), linearising constraints, increasing the sparsity of matrices, and tuning IPOPT. While the manual scaling did not yield any actual improvements, especially as there are no practical ways to scale second order derivatives, tuning IPOPT led to some measurable reductions of the convergence time. By choosing MA57 from the Harwell Subroutine Library[31] as a linear solver and the Metis package for matrix reordering,[32] the convergence time could be reduced to less than 25% in comparison to the default configuration.

Optimization of the *CPBMR*: Several operational and geometrical parameters of the *CPBMR* can be manipulated. The following 1 contains a comprehensive list of parameters of the *CPBMR* that may be modified within given bounds. For matters of problem size, additional possible decision variables are disregarded. Among those are the inlet pressures for shell- and tube-side, superficial velocities, and selection of the right type of catalyst. Similarly, the reactor length will be held constant at 20 cm, because of the difficulties related to removing or adding an entire heating/cooling segment, each of which is 10 cm long. The lower and upper bounds noted in 1 state what should be possible theoretically.

2 shows the configuration and the performance at the starting point (0), an intermediate step (1), and the final optimization results (2). $_L$ and ^{U} assign active lower or upper bounds on decision variables, which are specified by the user. Figure 5 shows the concentration profiles for ethylene and ethane and the temperature profile for the final optimization step noted in 2.

Table 1: Operational and geometrical parameters of the *CPBMR* that may be modified within the given bounds.

Parameter	**Symbol**	**Value**	**Lower bound**	**Upper bound**	**Unit**
Geometrical Parameters					
Diameter of tube	d_{tube}	0.007	0	d_{shell}	m
Diameter of shell	d_{shell}	0.010	d_{tube}	–	m
Membrane thickness	δ_{mem}	50	0.1	100	μm
Catalyst density	ρ_{cat}	3 600	0	3 700	kg/m^3
Catalyst volume fraction	φ_{cat}	0.64	0	1	–
Operational Parameters					
Temperature at inlet, shell-side	T^S_{Inlet}	1023.15	290	1375	K
Temperature at inlet, tube-side	T^T_{Inlet}	1023.15	290	1375	K
Cooling/heating temperature, seg. I	$T^I_{h/c}$	1023.15	290	1375	K
Cooling/heating temperature, seg. II	$T^{II}_{h/c}$	1023.15	290	1375	K
Molar fraction of oxygen, shell-side	$x^S_{O_2}$	0.128	0	1	–
Molar fraction of nitrogen, tube-side	$x^T_{CH_4}$	0.170	0	1	–

Table 2: Collection of decision variables for three steps in the optimization of the *CPBMR* and respective performance.

No.	T^{S}_{in} [K]	T^{T}_{in} [K]	$T^{\text{I}}_{\text{h/c}}$ [K]	$T^{\text{II}}_{\text{h/c}}$ [K]	$x^{\text{S}}_{O_2}$ [–]	$x^{\text{T}}_{CH_4}$ [–]
0	1023	1023	1023	1023	0.128	0.170
1	990_L	990_L	990_L	990_L	0.149^U	0.162_L
2	970_L	1013	970_L	970_L	0.157^U	0.128
No.	d_{T} [mm]	d_{S} [mm]	ρ_{cat} [kg/m^3]	φ_{cat} [–]	δ_{mem} [μm]	
0	7.0	10	3600	0.64	50	
1	6.0_L	7.8_L	3700^U	0.70^U	62.4	
2	6.0_L	7.8_L	3700^U	0.70^U	65^U	

No.	**Yield in C_2**	**Selectivity in C_2**	**Conversion of CH_4**
0	0.302 983	0.550 275	0.550 604
1	0.440 726	0.685 512	0.642 914
2	0.468 500	0.632 873	0.740 276

Selectivity Target

While having a high yield in C_2 products is advantageous, the product gas still needs to be cleaned of both reactants and side-products, like carbon oxides, before further processing. The selectivity

in C_2 hydrocarbons is a measure for how many of the reacted methane molecules formed hydrocarbons and how many carbon atoms went into the formation of carbon oxides: the lower the selectivity, the more carbon oxides are produced. The selectivities presented in the optimization results for the stand-alone operation of the *CPBMR* are already quite high ($\geq 60\%$). Nevertheless, it is examined to what extent it is possible to further increase the selectivity for a given optimal solution by enforcing a lower bound on the selectivity. As a starting point, the intermediate step 1 in 2 is chosen. The yield in C_2 hydrocarbons at that point lies at roughly 44% while the selectivity is just above 68.5%.

Apparently, an increase in the selectivity target of one percentage point does not cause the yield to drop by less than that amount. Yield decreases seem to be getting slowly larger when surpassing a selectivity of 75%. Only seven of the eleven decision variables stay at their original value comparing the starting point to the last step of the selectivity target optimization. The most obvious movement here is a shift to an even higher methane to oxygen ratio in the packed-bed as both methane fraction and membrane thickness go up while the oxygen fraction goes down.

Discussion of Results Before proceeding to the next step – the integration of the *CPBMR* into the membrane reactor network – a short discussion of all results so far is in order.

The performance of the *CPBMR* reported herein is – with respect to the yield in C_2 hydrocarbons – better than expected and reaches higher levels than have ever been experimentally found.

In order to simulate and optimize the *CPBMR* successfully, five radial and twelve axial finite elements are required. However, this system seems to be touching its boundaries in the last few optimization studies carried out here. It is possible that with an even larger number of radial finite elements an even better performance with respect to the yield in C_2 hydrocarbons could be reached.

The incorporation of radial effects into the *CPBMR* model makes a difference and is vital for obtaining more sensible results in comparison to the one-dimensional case. It is exactly this radial influence that makes the simulation and optimization of the *CPBMR* complicated as it is mainly

responsible for increasing the number of required variables by a factor of ten.

Overall, the general optimization of the *CPBMR* has confirmed some of the trends already found in a rough sensitivity analysis that was carried out on the decision variables:

1. There seems to be a general trend towards a thicker membrane. This obviously reduces the heat transfer between shell and tube, but the predominant effect seems to be the reduction of the molar flux of heavier molecules. Oxygen enters the tube through the membrane in the largest quantities, because of the large concentration difference between shell-side and tube-side. Consequently, the thicker the membrane the lower the oxygen flux, and thus, the lower the resulting oxygen concentrations in the reactor tube-side, which apparently ensure the highest possible yields. The oxygen levels found in simulations and optimizations of the *CPBMR* described above range between roughly zero and 500 Pa. What is interesting to see in this context is that there is – even at the outlet of the 20 cm long *CPBMR* – still a positive C_2 hydrocarbon formation rate. Common perception was that at that point the potential of methane conversion should be exhausted.

2. Inlet temperatures of both shell- and tube-side have dropped below the original 1 023.15 K and the cooling jacket is extracting some 28.5 W from the reactor in addition to the heat transported away by the shell-side stream while ensuring an almost isothermal temperature level in the tube-side of the *CPBMR*, and thus, allowing for optimal operating conditions along the entire reactor length as shown in Figure 5(c).

3. With respect to the catalytic bed, there seems to be a trend pointing at the minimization of the actual gas phase and covering as much of the packing with catalyst. However, this trend should not be overrated. A sensitivity analysis shows that the actual increase in the yield caused by this trend is comparatively small.

4. Another trend that has reemerged is the increasing dilution of the shell-side gas flow with nitrogen. This can be understood as a further move towards near-isothermal reactor operation as the higher dilution eases the exothermic effects of the reactions.

5. Lastly, a steady decline in the diameter of both tube and shell is observed. Obviously, this again has two beneficial effects: First of all, the total heat caused by the reaction is smaller. On a smaller diameter the heat transfer through the reactor shell is more effective.

Overall, it appears that the C_2 hydrocarbon production depends mostly on an optimal temperature control and the presence of a small amount of oxygen in the packed-bed. Economically speaking, however, there is a trade-off between a higher yield through dilution, diameter reduction, and the actual amount of C_2 hydrocarbons obtained in a reactor. Smaller reactors and higher dilution would require more reactors in total and thus more effort when it comes to the actual product separation. Finally, a few comments need to be made on some numerical issues:

1. After the intermediate step all further attempts to decrease the lower bounds on the temperatures have to be abandoned as the optimization just keeps running into either restoration phase failures or local infeasibilities.

2. The above noted optimization formulations and tasks required, in total, nearly three months to get to the last step.

3. For the last few tasks, the changes made to the variable bounds have to be chosen very carefully and the increases consequentially become ever smaller.

It should, be noted that all the conclusions so far should be handled with care. It is still questionable how accurate the model is and most of all to what extend Stansch's kinetics are in fact applicable in a conventional packed-bed membrane reactor.

There are of course a number of inaccuracies in the implemented reactor model apart from the margins of error of all applied transport and fluid parameter correlations. One issue, in particular, has to be revisited: One reason for the excellent performance of the *CPBMR* might be a questionable applicability of the kinetics developed by Stansch et al.[24] Their kinetics have been formulated based on experimental data from the application of the *OCM* process in a microcatalytic fixed-bed

reactor. As their reactor does not allow for continuous oxygen injection along the reactor length, the entire amount needs to be fed with methane. This obviously means that the oxygen concentrations at the inlet of the fixed-bed will always be higher than in a *PBMR*. Consequentially, Stansch et al. claim validity of their kinetics for oxygen partial pressures ranging from 1 kPa to 20 kPa. This can lead to some minor trouble in a fixed-bed reactor whenever oxygen is consumed by the reaction mechanism and drops below 1 kPa, but it is almost certainly an issue from inlet to outlet in a *PBMR*. In the conventional feeding-mode, no oxygen is being injected to the tube-side of the membrane reactor. The only oxygen in the reactor tube-side arrives there by permeating the membrane from the shell-side. Accordingly, the oxygen partial pressure will always stay at quite low levels. In fact, it has been observed that whenever methane conversion is close to or larger than 50% in the *CPBMR* model, the oxygen level at every single collocation position is well below 1 kPa ranging from 0 to 500 Pa. As the parameters of the kinetics were not fitted for this range of partial pressures, it can easily be imagined that this leads to an overestimation (or possibly underestimation) of the reactor performance. Given how a *PBMR* works, there is however no way to guarantee oxygen levels of more then 1 kPa in the fixed-bed – at least with this kinetic system. A closer look at the formation rates of all components for those low partial pressures of oxygen shows indeed a maximum for the formation of C_2 hydrocarbons for temperatures above 1000 K, well below 1000 Pa of oxygen. For details on this behaviour see Figure 6 This, by no means, invalidates the kinetic system, but shows that a thorough experimental investigation is required.

Operation of the Membrane Reactor Network

This section deals with the simulation and optimization of the membrane reactor network shown in Figure 1. After a brief description of the implementation of the one-dimensional models for the *FBR* and the *PPBMR*, this part goes on by presenting some details on how those two and the *CPBMR* are going integrated into the *MRN*. Lastly, details on the attempted general optimization of the *MRN* will be presented. In addition, the assumption, that one-dimensional models for both

FBR and *PPBMR* suffice, is revisited by comparing their results against two-dimensional models.

Implementation of Models for *FBR* and *PPBMR*: The *FBR* is expected to be considerably shorter than the *CPBMR*. Hence, only one heating/cooling segment is introduced. Methane and oxygen need to be fed to the reactor at the same inlet. Consequently, the concentration profiles can be expected to be steeper and temperature hot spots could be more of a problem. This basically means that the length of individual finite elements needs to be a lot smaller and that more axial finite elements are required in comparison to the *CPBMR*. Keeping the temperature in the reactor in check is a bit more of a challenge compared to the CPBRM as feed dilution with nitrogen gas of more than 80% together with a catalyst dilution of one to four was necessary in previous work.[33] It appears that the heat transfer through the outer shell is even more important in the *FBR* compared to the *CPBMR*. It is found that especially oxygen disappears quite quickly, when the temperature level gets out of control. Moreover, the axial derivative becomes so large that for longer finite elements negative oxygen values are unavoidable as the collocation is incapable of accurately following that decline. Apart from being unacceptable, the temperature increase is also contradictory to the aim of achieving high yields in C_2 hydrocarbons. For a feed dilution of 85%, methane conversion climbs to roughly 62.5%, however, selectivity is so low that there is close to no yield in C_2 products at all. For a 87% dilution, this is fairly different: Methane conversion is half as high at 33.8% and the yield in C_2 around 7.6%. The sudden formation of hot spots needs to be taken into account as this requires a denser discretization. As a starting point, 1 cm of reactor length will be discretized with 100 axial finite elements each 10^{-4} m long. The higher oxygen levels in the tube-side of the *PPBMR* cause the same trouble as in the *FBR*, meaning that yet again a higher number of finite elements is required, which need to be quite short. The *PPBMR* in the *MRN* sits right behind the *FBR*. Some additional oxygen and nitrogen is added to the flow leaving the *FBR* before entering the *PPBMR*, but for now the concentrations of the flow leaving the *FBR* will simply be reused for the inlet of the tube of the *PPBMR*. The required dilution with nitrogen found here is obviously quite high. This is, however, not necessarily unexpected. The best yield

in C_2 hydrocarbons experimentally reported so far requires a dilution of methane with helium of 98% while allowing for a yield of 35% and a selectivity of 54% in a membrane reactor using a $Bi_{1.5}Y_{0.3}Sm_{0.2}O_{3-\Delta}$-catalyst,.[35] Figures 7 and 8 show the concentration profiles for the reaction zones of both reactors at a feed dilution of 87%.

Integration of *FBR*, *PPBMR*, and *CPBMR*: For practical reasons, the network has basically only two different feed streams: the first containing methane, the second oxygen. Both gases will be diluted with nitrogen. This means that streams 2, 11, and 14 (see 1) consist of the same molar fractions of oxygen and nitrogen, streams 1, 9, and 6 of the same molar fractions of methane and nitrogen. As a starting point and to get a good match with the previously done simulations of *FBR* and *PPBMR*, each stream is diluted to a molar fraction of nitrogen of 87%. Because of recycle stream number 7 from *PPBMR* shell-side to *CPBMR*, tube-side superficial velocities in both *FBR* and *PPBMR* are reduced to 0.4 m/s to ensure that the same can stay below or at 1 m/s in the *CPBMR*. The heating/cooling temperature in the *CPBMR* is slightly decreased to 950 K to prevent possible problems as a consequence of recycle stream no. 7 from the shell-side of the *PPBMR* to the tube-side of the *CPBMR*. Similarly, as a further precaution, the shell-side inlet temperature of the *PPBMR* is decreased to 900 K. Both stream 14, which is initally set to zero, and recycle stream 12, which will be activated to just 5% of its possible flow, can increase the oxygen concentration in the tube-side of the *PPBMR*, and thus, strengthen exothermic reactions. 3 contains the results of the network simulation for the configuration described above.

Table 3: Results of the *MRN* simulation.

Component	**Yield in C_2 Products**	**Selectivity in C_2 Products**	**Conversion of Methane**
FBR	0.047 666	0.194 696	0.244 823
PPBMR	0.008 562	0.142 233	0.060 195
CPBMR	0.418 325	0.603 931	0.692 669
MRN	0.293 901	0.430 539	0.682 637

This point is obviously far from being an optimal solution as both methane conversion and yield in

C_2 hydrocarbons of the network are lower than those for the individual *CPBMR*. Nevertheless, it is a good starting point in order to show that the network model actually works. The *CPBMR* in the network is probably close to the optimal solution found in the stand-alone optimization, because of the high dilution with nitrogen required by the other two reactors. The reduction of the superficial velocity in the *FBR* causes the temperature in that particular reactor to drop very quickly, thus, reducing the reaction rates to nearly zero after the first 2 mm of reactor length. The situation in the *PPBMR* is quite similar, although the reaction rates do not become completely zero before the reactor end.

General Optimization of the *MRN*: For the general optimization of the MRN, all geometrical and operational parameters mentioned for the CPBMR can be manipulated. In addition, more or less the same parameters are relevant for the other two reactors. The network itself offers some additional decision variables through the manipulation of recycle streams and the two feed streams. Initial sensitivity analyses at the afore-mentioned starting point show the appearance of numerous (local) infeasibilities brought along by the additional two reactors. Generally speaking, only the improvements described for the CPBMR above led to any improvements in the yield of C_2 hydrocarbons for the entire network. The sensitivity analysis would imply removing the additional reactors. However, this could simply be because of the excellent performance of the CPBMR at the starting point.

Further Investigation of *FBR* and *PPBMR*: The investigation on the CPBMR shows the necessity of its corresponding two-dimensional model. Given the size and complexity of the model for the MRN, only one-dimensional models are first used for the additional reactors. In order to further examine the implications of this simplification, two-dimensional models for both FBR and PPBMR are implemented. Even after a few millimetres of reactor length, the results of one- and two-dimensional models deviate by several percentage points. The simultaneous feeding of oxygen and methane to the catalytic packed-bed leads to the formation of a hot-spot in the reactor center, which cannot be seen in the one-dimensional case. In the case of the FBR, it might be

possible to tune the behaviour of the 1D system to the 2D, provided that the temperature can be controlled more effectively. The latter is not possible for the PPBMR. The diffusive flux through the membrane, yet again, necessitates the second dimension. A two-dimensional model for the entire MRN amounts more than half a million variables and cannot be solved in a timely manner using available hardware.

Conclusions and Outlook

Simulations carried out as part of this work show that using a two-dimensional instead of just a one-dimensional model for the *CPBMR* is necessary and makes quite a difference at higher methane conversion rates, although previously carried out research in this field[36] suggested the difference maybe rather small. The advantages of the *CPBMR* in contrast to the *FBR* have become fairly obvious here. As was proven in the selectivity target investigation, it is possible to ensure both high yields of more than 40% and selectivities of more than 70% at the same time. The fairly small influx of oxygen through the membrane prevents side-reactions and helps keep the temperature increase in check at the same time. In addition, the influence of a heating/cooling system on the *CPBMR* has been tested. The configuration implemented here in combination with the feed dilution allows for almost isothermal temperature profiles in the reactor. These very helpful operating conditions can, however, not be implemented in *FBR* and *PPBMR*. The higher oxygen concentrations in the catalytic bed lead to barely controllable temperature spikes causing the oxygen to react fairly quickly and causing low yields in C_2 hydrocarbons. Further studies show that the radial temperature dependence cannot *a priori* be neglected in the *FBR* and is almost certainly an issue in the *PPBMR* because of the insulating effect of the shell-side.

All the previously drawn conclusions were made under the assumption of applicability for Stansch's kinetics. However, all results obtained for the *CPBMR* lie in a range for which Stansch et al. do not claim validity for their kinetics. The partial pressure of oxygen simulated in the tube-side of the *CPBMR* lies well below their lower bound of 1000 Pa between 0 and 500.

Therefore, an important topic for our current research work represents an examination of the applicability of the reaction kinetics applied here. Experiments are on the way so as to test the operating conditions with high yields and selectivities and to distinguish to what extent they are reasonable. For example, Schomäcker et al.[37] discover that lattice oxygen of a vanadium oxide catalyst plays a greater role at low oxygen pressures. Therefore, the intermediate reduction of the catalyst might influence the selectivity of the reaction mechanism.

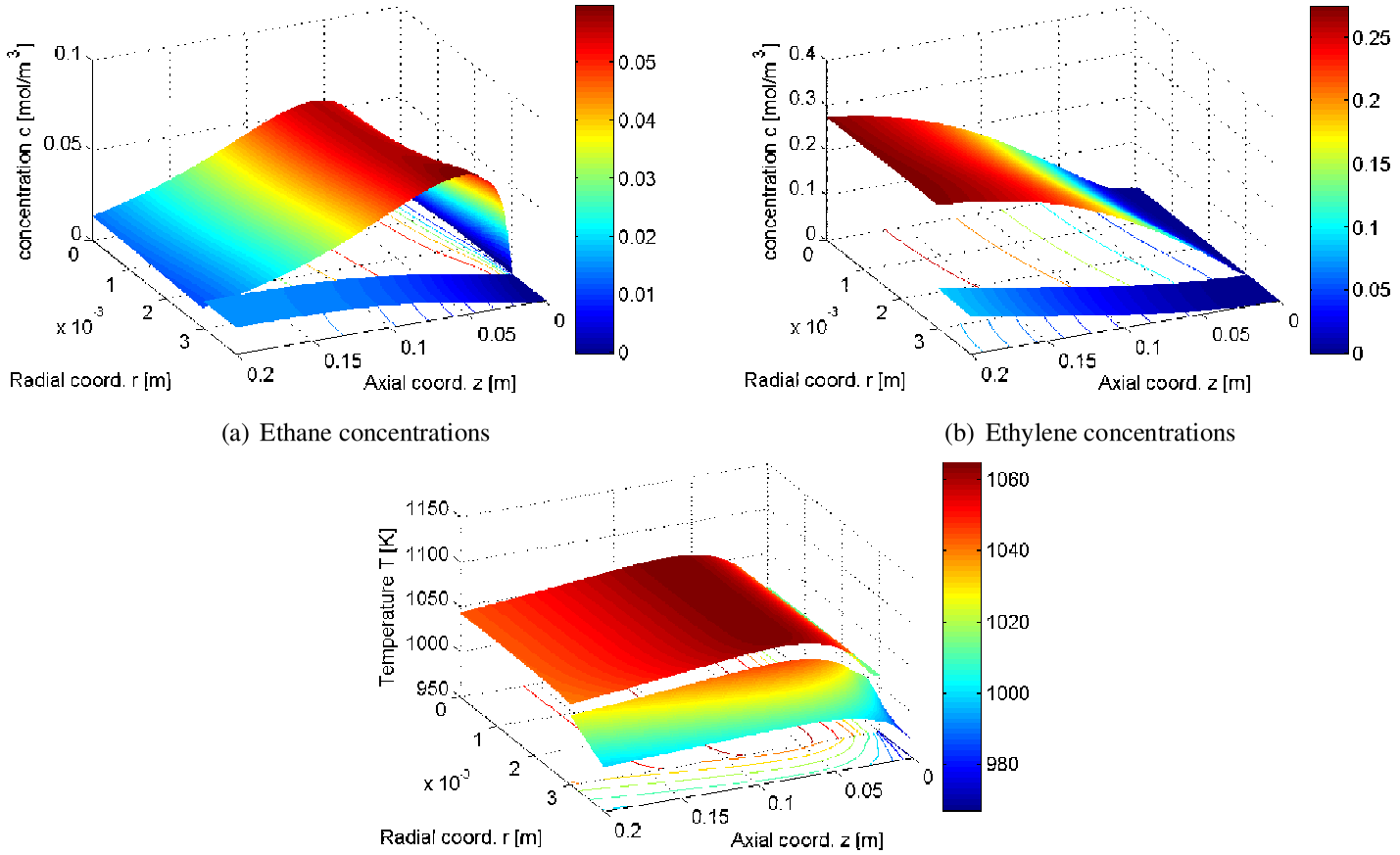

(a) Ethane concentrations

(b) Ethylene concentrations

(c) Temperature profile

Figure 5: Ethane, ethylene and temperature profiles for the last step of the *CPBMR* stand-alone optimization.

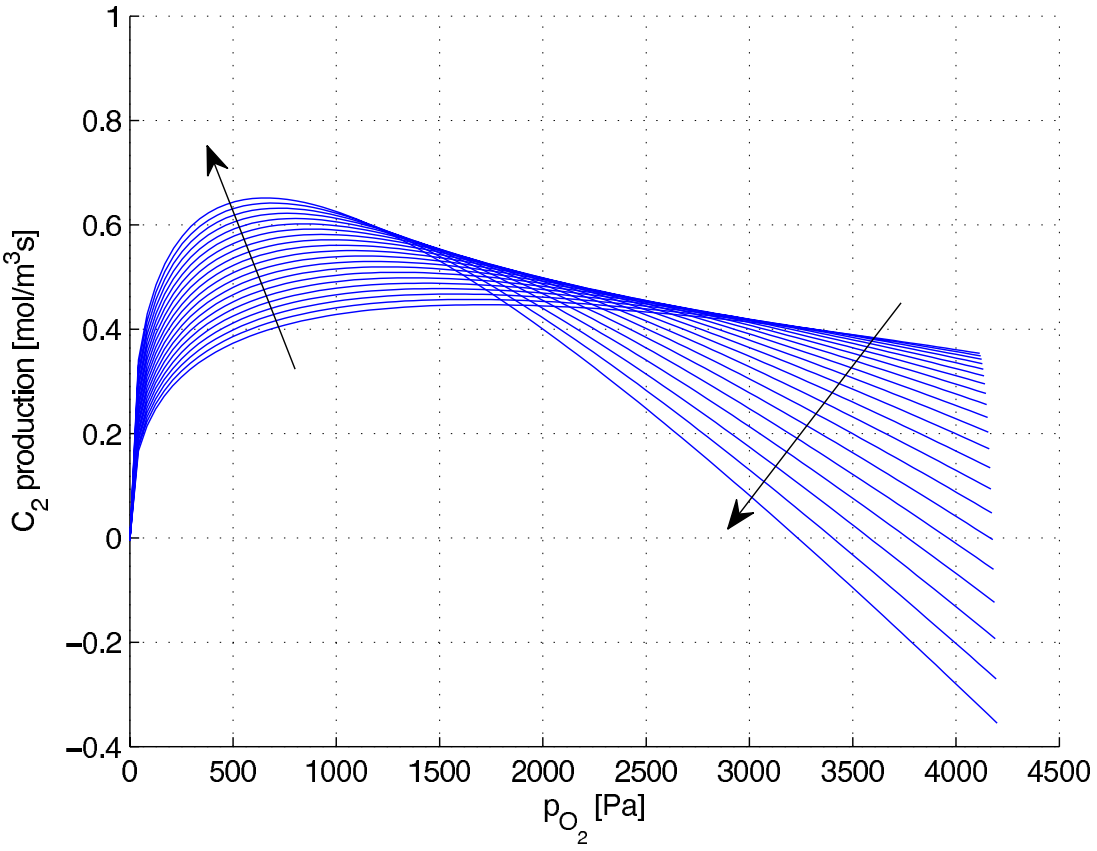

Figure 6: Rate of formation of C_2 products for various partial pressures of oxygen and different temperature levels.

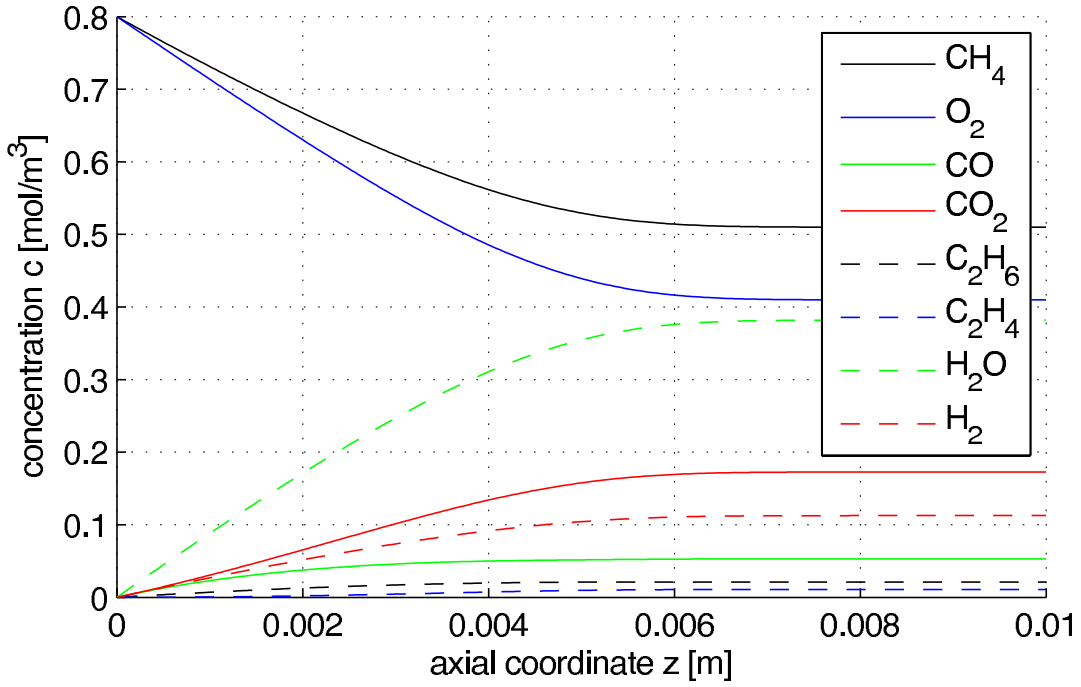

Figure 7: Concentration profiles for the FBR using a feed dilution of 87%.

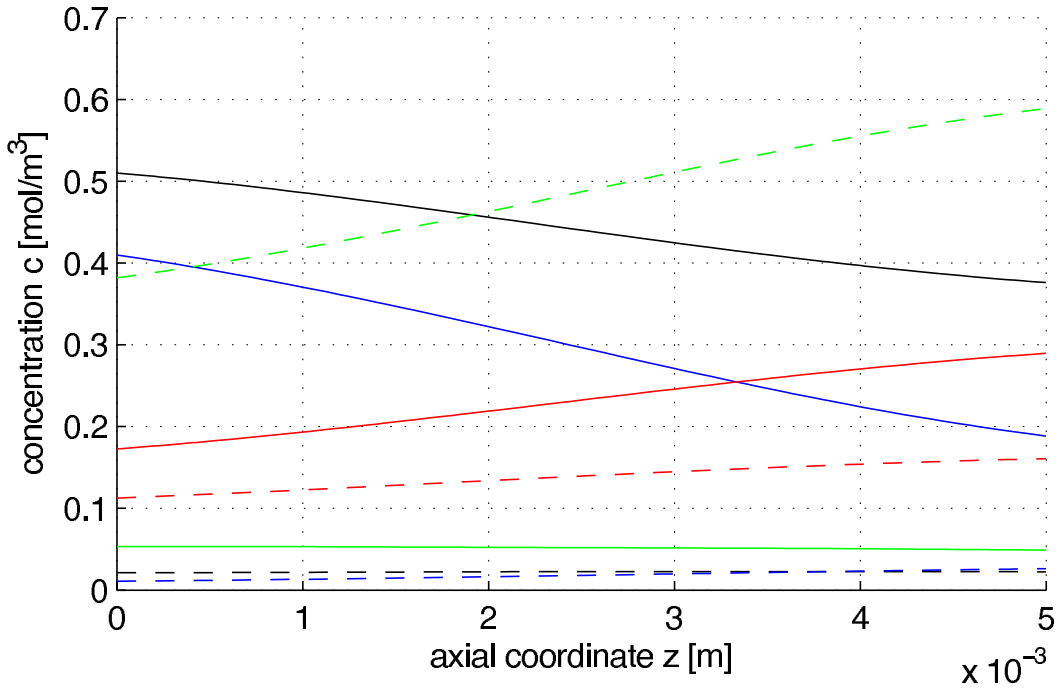

Figure 8: Concentration profiles for the PPBMR tube-side using a feed dilution of 87%. For details on which line symbolizes which component, please refer to 7.

Notation

Nomenclature

Symbol	Meaning	Unit	Explanations/Comments
c	concentration	mol/m^3	
c_p	specific heat capacity	kJ/kg K	
$\dot{cr}$	component rate	mol/m^3 s	
$\dot{h}$	enthalpy flux	W/m^2	area specific enthalpy flow
k	heat transfer coefficient	W/m^2 K	
ℓ	Lagrangian polynomial	–	
$\dot{q}$	heat flux	W/m^2	area specific heat flow
r	radius, radial coordinate	m	
$\dot{r}r$	reaction rate	mol/m^3 s, mol/g s	conversion rate of reactions, differs between gas phase and surface reactions
t	time	s	
u_z	superficial velocity	m/s	
z	axis, axial coordinate	m	
$\mathscr{D}$	diffusion coefficient	m^2/s	
$\mathscr{H}$	Hermite polynomial	–	
$\dot{N}$	molar flow	mol/s	
T	temperature	K	
φ	volume fraction	–	
λ	thermal conductivity	W/m K	
ρ	density	kg/m^3	
$_{i,j,k}$	index variables		walk through components or reactions
$_r$	radially		
$_{\text{cat}}$	catalyst		
$_{\text{cool}}$	variable belongs to heating/cooling system		
$_{\text{diff}}$	diffusion		
$_{\text{mix}}$	mixture		
$_{\text{shell}, S}$	shell-side		
$_{\text{tot}}$	total		e.g. sum or average over all species
$_{\text{trans}}$	transfer		e.g. heat transfer through a membrane
$_{\text{tube}, T}$	tube-side		
$_G$	gas		
$_{OS}$	outer shell		
CPBMR	coventional packed-bed membrane reactor		packed-bed membrane reactor with a conventional feeding policy
FBR	fixed-bed reactor		
MRN	membrane reactor network		network consisting of *FBR*, *CPBMR*, and *PPBMR*
PBMR	packed-bed membrane reactor		
PPBMR	proposed packed-bed membrane reactor		membrane reactor with an alternative feeding policy

Notes and References

1. Unruh D, Pabst K, Schaub G. Fischer-Tropsch Synfuels from Biomass: Maximizing Carbon Efficiency and Hydrocarbon Yields. *Energy Fuels*. 2010;24:2634 – 2641.

2. Jašo S, Godini H, Arellano-Garcia H, Omidkhah M, Wozny G. Analysis of attainable reactor performance for the oxidative methane coupling process. *Chemical Engineering Science*. 2010;65:6341 – 6352.

3. Lafarga D, Santamaría J, Menéndez M. Methan Oxidative Coupling Using Porous Ceramic Membrane Reactors – I. Reactor Development. *Chemical Engineering Science*. 1994; 49(12):2005 – 2013.

4. Quddus MR, Zhang Y, Ray AK. Multiobjective Optimization of a Porous Ceramic Membrane Reactor for Oxidative Coupling of Methane. *Ind Eng Chem Res*. 2010;49:6469 – 6481.

5. Ref. 4, p. 6469.

6. Chan PYP. Design and Verification of Catalytic Membrane Reactor for H_2 Recovery from H_2S. Ph.D. thesis, The University of New South West Wales – The School of Chemical Science and Engineering, Sydney, Australia. 2007.

7. Ref. 6, p. 17ff., 46ff.

8. Godini H, Arellano-Garcia H, Omidkhah M, Karimzadeh R, Wozny G. Model-Based Analysis of Reactor Feeding Policies for Methane Oxidative Coupling. *Ind Eng Chem Res*. 2010; 49:3544 – 3552.

9. Jašo S, Godini H, Arellano-Garcia H, Wozny G. Oxidative Coupling of Methane: Reactor Performance and Operating Conditions. In: *20th European Symposium on Computer Aided Process Engineering – ESCAPE 20*, edited by Perucci S, Ferraris GB. 2010; .

10. und Chemieingenieurwesen (GVC) VDIVGV, ed. *VDI-Wärmeatlas*. Springer-Verlag Berlin Heidelberg, 10th ed. 2006.

11. Fuller EN, Schettler PD, Giddins JC. A New Method For Prediction of Binary Gas-Phase Diffusion Coefficients. *Industrial And Engineering Chemistry*. 1966;58(5):18 – 27.

12. Kee RJ, Coltrin ME, Glarborg P. *Chemically Reacting Flow*. Wiley-Interscience. 2003.

13. Ref. 12, p. 528.

14. Tsotsas E, Schlünder EU. On Axial Dispersion in Packed Beds with Fluid Flow. *Chemical Engineering and Processing*. 1988;24(1):15 – 31.

15. Tóta Á, Hlushkou D, Tsotsas E, Seidel-Morgenstern A. Packed-bed Membrane Reactors. In: *Modeling of Process Intensification*, edited by Keil FJ, chap. 5, pp. 99 – 148. WILEY-VCH Verlag GmbH & Co. KGaA. 2007;.

16. Ref. 15, p. 117.

17. Ref. 3, p. 2011.

18. Ref. 10, p. Da 26.

19. Poling BE, Prausnitz JM, O'Connell JP. *The Properties of Gases and Liquids*. McGraw-Hill. 2001.

20. Bauer R, Schlünder EU. Effective radial thermal conductivity of packing in gas flow. Part I. Convective transport coefficient. *Int Chem Eng*. 1978;18(2):181 – 188.

21. Bauer R, Schlünder EU. Effective radial thermal conductivity of packing in gas flow. Part II. Thermal conductivity of the packing fraction without gas flow. *Int Chem Eng*. 1978;18(2):189 – 204.

22. Specchia V, Baldi G, Sicardi S. Heat Transfer in Packed Bed Reactors With One Phase Flow. *Chem Eng Commun*. 1980;4:361 – 380.

23. Dixon AG. Wall And Particle-Shape Effects on Heat Transfer in Packed Beds. *Chem Eng Comm*. 1988;71:217 – 237.

24. Stansch Z, Mleczko L, Baerns M. Comprehensive Kinetics of Oxidative Coupling of Methane over the La_2O_3/CaO Catalyst. *Ind Eng Chem Res*. 1997;36:2568 – 2579.

25. Biegler LT. *Nonlinear Programming – Concepts, Algorithms, and Applications to Chemical Processes*. Philadelphia, Pennsylvania: SIAM Society for Industrial and Applied Mathematics & MOS Mathematical Optimization Society. 2010.

26. Ref. 25, p. 288ff.

27. Finlayson BA. *Nonlinear Analysis in Chemical Engineering*. McGraw-Hill International Book Company. 1980.

28. Ref. 27, p. 272.

29. Wächter A, Biegler L. On the implementation of an interior-point filter line-search algorithm for large-scale nonlinear programming. *Math Program*. 2005;Ser. A.

30. Ref. 25, p. 151 ff.

31. Hogg J. HSL Mathematical Software Library. `http://www.hsl.rl.ac.uk/`. 2011.

32. Karypis G, Kumar V. METIS – Graph Partioning, Mesh Partioning, Matrix Reordering. `http://people.sc.fsu.edu/\~jburkardt/c\_src/metis/metis.html`. 2006.

33. Ref. 2, p.6350, fig. 17.

34. Caro J. Membranreaktoren für die katalytische Oxidation. *Chemie Ingenieur Technik*. 2006; 78(7):899 – 912.

35. Ref. 34, p.908.

36. Glöser S. *Zweidimensionales Simulationsmodell für einen Membranreaktor zur oxidativen Kopplung von Methan*. Technische Universität Berlin - Fachgebiet Anlagen- und Sicherheitstechnik. 2010.

37. Dinse A, Schomäcker R, Bell AT. The role of lattice oxygen in the oxidative dehydrogenation of ethane on alumina-supported vanadium oxide. *Physical Chemistry Chemical Physics*. 2009; 11:6119 – 6124.

List of Figures

1 Flowsheet of the proposed membrane reactor network. Figure redrawn in accordance with.[8] 3
2 Balance volume for the derivation of the isothermal model for the *CPBMR*. 6
3 Sketch for the heated or cooled model of the *CPBMR* 7
4 Depiction of the collocating surface function using Hermite and Lagrangian polynomials and the meaning of respective collocation variables. 10
5 Ethane, ethylene and temperature profiles for the last step of the *CPBMR* standalone optimization 22
6 Rate of formation of C_2 products for various partial pressures of oxygen and different temperature levels. 23
7 Concentration profiles for the FBR using a feed dilution of 87%. 24
8 Concentration profiles for the PPBMR tube-side using a feed dilution of 87%. For details on which line symbolizes which component, please refer to 7. 24

List of Tables

1 Operational and geometrical parameters of the *CPBMR* that may be modified within the given bounds. 12
2 Collection of decision variables for three steps in the optimization of the *CPBMR* and respective performance. 12
3 Results of the *MRN* simulation 18